New Journal of Physics
The open access journal at the forefront of physics

Deutsche Physikalische Gesellschaft DPG
IOP Institute of Physics

Published in partnership with: Deutsche Physikalische Gesellschaft and the Institute of Physics

OPEN ACCESS

RECEIVED
14 February 2022

ACCEPTED FOR PUBLICATION
29 March 2022

PUBLISHED
25 April 2022

PAPER

Majorana-like end states in one-dimensional dimerized Kitaev topolectrical circuit

Junjie Yao[1], Xiamin Hao[1], Biyu Song[1,2], Yizhen Jia[1,2], Chenqiang Hua[2] and Miao Zhou[1,2,*]

[1] School of Physics, Beihang University, Beijing 100191, People's Republic of China
[2] Beihang Hangzhou Innovation Institute Yuhang, Hangzhou 310023, People's Republic of China
[*] Author to whom any correspondence should be addressed.

E-mail: mzhou@buaa.edu.cn

Keywords: topolectrical circuit, Kitaev chain, band structures, Majorana splitting, topological phase transition

Supplementary material for this article is available online

Abstract

Majorana zero modes (MZMs) have attracted tremendous attention in condensed matter and materials physics communities due to the implications in topological quantum computation. One-dimensional (1D) dimerized Kitaev chain is a prototype model for MZMs, but its realization remains a challenge in material systems. Here, we develop a distinctive approach to achieve Majorana-like end states (MESs) by implementing practical dimerized Kitaev topolectrical circuits. Specifically, two arrays of inductors are arranged to simulate particles and antiparticles, while intra- and inter-array capacitive connections are used to model hopping and superconducting pairing. Three topological phases can be achieved by tuning the capacitance, i.e. the trivial phase, Su–Schrieffer–Heeger topological phase and Kitaev phase, with distinct field strength distributions in real space. Majorana splitting is observed around a domain wall in the circuit, and we propose an efficient experimental observable-edge distance-to characterize the process as premonition of topological phase transition. Remarkably, dynamics of the Gaussian wave packet in time domain provide an excellent signal to detect MESs in experiments, as only MESs allow nonlocal propagation in circuit network. Our results not only manifest the superiorities of topolectrical circuits for exotic topological states, but also pave the way for possible applications in electrical engineering and signal processing.

1. Introduction

During the past decade, tremendous efforts have been made in the search of various exotic topological states of matter, including but not limited to topological insulators, Dirac/Weyl semimetals, topological nodal line semimetals, and topological superconductors (TSCs) [1–6]. Realization of TSCs that support Majorana zero modes (MZMs) is an exciting topic of both fundamental scientific importance and technological potential applications, as MZMs are regarded as promising candidates for fault-tolerant quantum computing [7, 8]. MZMs correspond to neutral excitations comprised of an equal superposition of electrons and holes. The unique properties of Majorana quasiparticles lie in the fact that they are their own antiparticles, closely related to Majorana fermions that exhibit an extensive ground-state degeneracy and non-abelian exchange statistics. So far, a few material systems have been put forward for observing MZMs, such as the interface between topological insulators and superconductors [9–11], semiconductors with strong spin–orbit coupling (SOC) [12–15], phase-biased Josephson junctions [16] and magnetic atomic chains [17, 18].

Physically, there are three basic ingredients for MZMs: superconducting proximity effect, a spin-rotation mechanism (most commonly SOC) and time-reversal symmetry breaking [6]. By fine-tuning these ingredients, the energy bands near Fermi level become effectively spinless, lifting the Karamer's degeneracy,

while the superconducting pairing remains achievable. In practice, among all the material systems proposed, the one-dimensional (1D) proximitized nanowires have been considered as the most promising platform for MZMs [14, 19–28]. However, plenty of experiments suggested that the SOC energy scale is still too small to trap MZMs (e.g. ∼1 K for InAs/InSb nanowires) [19–24]. More importantly, it remains a challenge to fabricate large-scale TSC nanowires and characterize MZMs due to the intrinsic instability and sophisticated experimental techniques, including the zero-bias tunneling and Coulomb blockade measurements [29, 30]. Therefore, it is highly desirable to search for alternative physical systems to achieve MZMs.

In this contribution, we theoretically introduce a topolectrical circuit and demonstrate the realization of Majorana-like end states (MESs) in circuit systems. It should be noted that electrical circuits are classical systems and cannot simulate TSC due to the lack of particle–hole symmetry. Nevertheless, MESs exhibit intriguing physical properties that can simulate the braiding behavior of Majorana fermions [31]. Recent reports showed that electrical circuits provide a powerful platform to simulate a plethora of exotic topological quantum states [32–35], even of higher-orders/dimensions [36–38]. By using simple inductors and capacitors, we construct a specific circuit network to simulate the 1D dimerized Kitaev chain. The dimerized Kitaev chain is the prototype model for spinless p-wave TSCs, in which the competition between Su–Schrieffer–Heeger (SSH) order and Kitaev order gives rise to a rich phase diagram [39]. However, so far there are no practical systems that can host this model due to the complexity of the dimerized Kitaev structure. We arrange two arrays of inductors to simulate particles and antiparticles, while intra- and inter-array connections can be used to simulate hopping and superconducting pairing. By tuning the capacitance, three distinct topological phases emerge in the circuit, including the trivial phase, SSH topological phase and Kitaev phase, which manifest different band structures and field strength distributions. Interestingly, Majorana splitting can be induced by increasing the superconducting pairing strength that fosters the topological phase transition from trivial to Kitaev phase, where the field strength peak at the domain wall splits into two peaks located at two ends of the circuit chain, and an experimental observable-edge distance-is proposed to facilitate the detection. We further investigate the dynamics of Gaussian wave packet in time domain, and demonstrate that MESs realized in the topolectrical circuit allow nonlocal propagation of wave packet throughout the circuit, which may greatly benefit the experimental observation.

2. Model and methodology

We begin with the tight-binding model of the 1D dimerized Kitaev chain as schematically depicted in figure 1(a). The Hamiltonian can be written as [39],

$$\begin{aligned} H = & -\mu \sum_i (c^\dagger_{A,i} c_{A,i} + c^\dagger_{B,i} c_{B,i}) \\ & - t \sum_i [(1+\eta) c^\dagger_{B,i} c_{A,i} + (1-\eta) c^\dagger_{A,i+1} c_{B,i} + \text{H.c.}] \\ & + \Delta \sum_i [(1+\eta) c^\dagger_{B,i} c^\dagger_{A,i} + (1-\eta) c^\dagger_{A,i+1} c^\dagger_{B,i} + \text{H.c.}], \end{aligned} \tag{1}$$

where i is the index of unit cell with A/B denoting the sublattice coordinate. μ is the chemical potential and t is the electron hopping term. Δ and η represent the p-wave superconducting pairing amplitude and the dimerization parameter, respectively. As such, the Hamiltonian harbors characteristics of both SSH and Kitaev models [40, 41]: with $\mu = 0$ and $\Delta = 0$, it reduces to SSH model, and with $\eta = 0$ it is Kitaev type.

In the dimerized Kitaev chain, TSCs may appear and the MZMs at two ends can be determined by solving the Bogoliubov–de Gennes (BdG) equation. By diagonalizing the BdG Hamiltonian matrix, the eigenstates is obtained. With the four-component operator $C^\dagger_k = (c^\dagger_{kA}, c^\dagger_{kB}, c_{-kA}, c_{-kB})$, the BdG Hamiltonian H_{BdG} in momentum space (k space) is expressed as,

$$H_{\text{BdG}} = \frac{1}{2} \sum_k C^\dagger_k H(k) C_k, \tag{2}$$

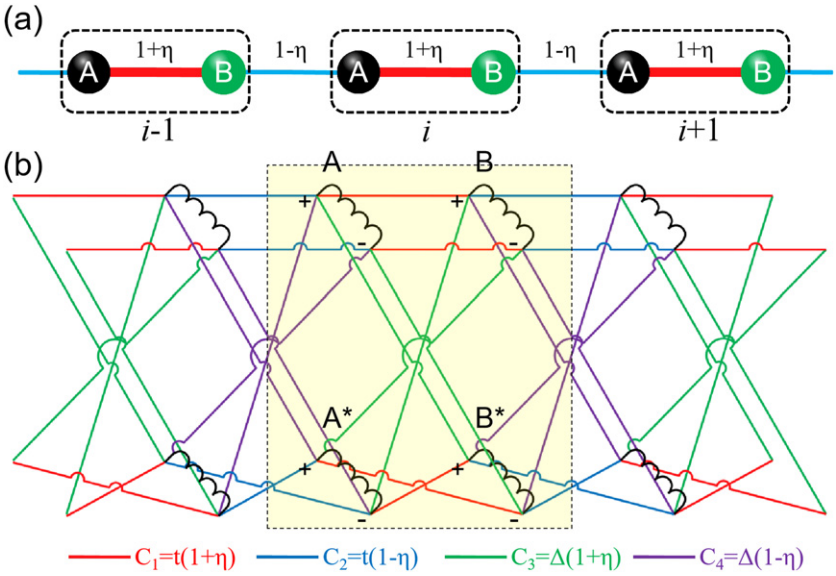

Figure 1. Dimerized Kitaev model and its circuit implementation. (a) Illustration of the dimerized Kitaev chain. The *i*th unit cell is indicated by the black dashed box. *A*/*B* is the sublattice, and the dimerization is indicated by different hopping (red and blue lines). (b) Circuit implementation of the dimerized Kitaev chain, in which two arrays of inductors are arranged to resemble particles and antiparticles.

with

$$H(k) = \begin{pmatrix} -\mu & z & 0 & w \\ z^* & -\mu & -w^* & 0 \\ 0 & -w & \mu & -z \\ w^* & 0 & -z^* & \mu \end{pmatrix}, \tag{3}$$

where

$$z(k) = -t[(1+\eta) + (1-\eta)\mathrm{e}^{-\mathrm{i}ks}], \tag{4}$$

$$w(k) = -\Delta[(1+\eta) - (1-\eta)\mathrm{e}^{-\mathrm{i}ks}], \tag{5}$$

where s denotes the distance between adjacent sites.

We then consider the practical circuit implementation of the dimerized Kitaev chain. As shown in figure 1(b), the designed circuit involves two arrays of inductors within a LC network. Each unit cell contains four sublattices (A, B, A* and B*) and each sublattice is simulated by an inductor. We define $U_a = U_{a+} - U_{a-}$ as the voltage across an inductor, with a representing the four inductors, and $+/-$ the two ends of an inductor. Parallel ($+$ to $+$ and $-$ to $-$) or antiparallel ($+$ to $-$ and $-$ to $+$) connection can be used to realize positive or negative coupling. It is able to define the top array as particles and the bottom array as antiparticles, so that the hopping terms can be simulated by connections between inductors within the same array using capacitors with capacitance $t(1 \pm \eta)$, while superconducting pairing is simulated by inter-array connections using capacitors with capacitance $\Delta(1 \pm \eta)$. Therefore, different from previous proposal in using node voltage as the basis of wave function and circuit Laplacian to solve the impedance distribution [31], here we employ the voltage difference across an inductor as the basis of wave function and the dynamic equation to describe the dynamics of field strength distribution.

The dynamic properties of this circuit can be analyzed by using Kirchhoff's law. The detailed derivation can be found in note in supplementary material (https://stacks.iop.org/NJP/24/043032/mmedia). Here we only present the dynamic matrix of the circuit, and the equation of motion in k space is written as,

$$\frac{1}{\omega^2} U_k = M_k U_k, \tag{6}$$

$$M_k = \frac{L}{2} \times \begin{pmatrix} m_0 - \mu & z & 0 & w \\ z^* & m_0 - \mu & -w^* & 0 \\ 0 & -w & m_0 + \mu & -z \\ w^* & 0 & -z^* & m_0 + \mu \end{pmatrix}, \tag{7}$$

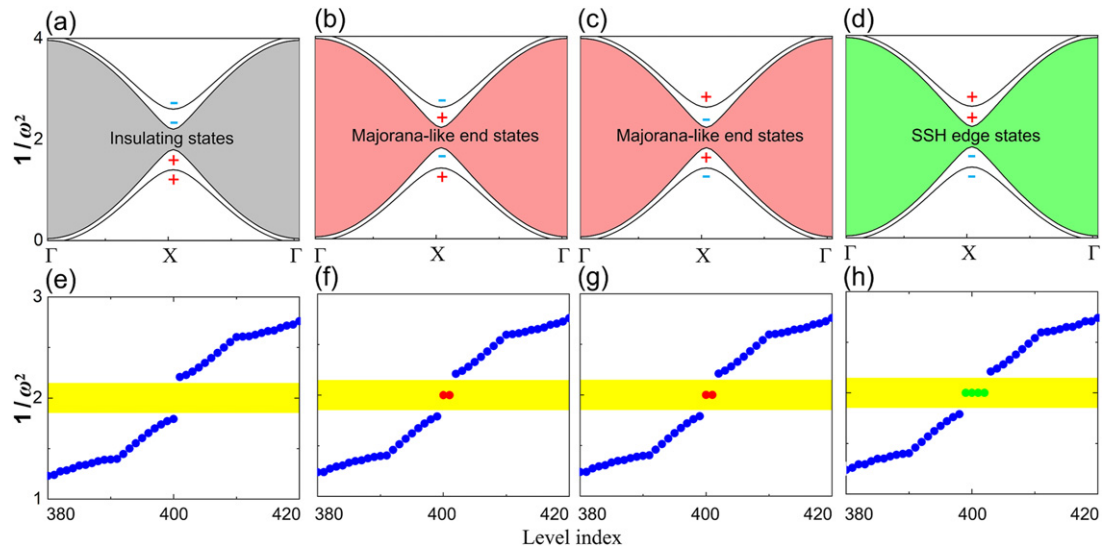

Figure 2. Band structures for infinite and finite LC chains. (a)–(d) Band structures for an infinite dimerized Kitaev circuit of different topological phases, (a) the trivial phase with $\eta = 0.2$, (b) Kitaev phase with $\eta = 0.05$, (c) Kitaev phase with $\eta = -0.05$, and (d) SSH topological phase with $\eta = -0.2$. For all cases, $\Delta = 0.1$. The calculated parities at X point are also indicated. (e)–(h) Discrete energy levels of a finite circuit chain with 200 unit cells corresponding to (a)–(d). The MESs and SSH edge states are highlighted within the bulk gap.

where $U_k \equiv (U_A, U_B, U_{A^*}, U_{B^*})^{\mathrm{T}}$ with T the transpose symbol and ω the excitation frequency. Clearly, the circuit dynamic matrix is similar to the tight-binding matrix, except that the on-site potential is described by m_0, and there is a constant coefficient $L/2$ that is attributed to inductors. The opposite chemical potentials of particles and antiparticles are realized by using different grounding capacitors between the top and bottom arrays. It should be noted that the eigenvalue of M_k is $1/\omega^2$ because the magnitude of matrix elements (expressed by the product of inductance and capacitance) corresponds to resonant frequency in LC circuits, similar to the energy in electronic systems. Without losing generality, L and t are set to 1.

3. Results and discussion

3.1. Topological band structures for the infinite and finite LC chain

The calculated band structures for an infinite LC chain with different capacitance are displayed in figures 2(a)–(d), with the detailed band evolution and phase diagram presented in figure S1 in note in the supporting information. There are four bands with an energy gap at X point, and the band shape looks similar with different capacitance. To explore the topological properties, we computed the parities of the wave functions for these energy bands. As the band gap closes and reopens at X point, we focus on the parities at this point, labeled by '+' and '−' in the figure. When η is positive with $\eta > \Delta$, the parities of the top two bands are '−' and the bottom two bands are '+', corresponding to a SSH-like trivial phase (figure 2(a)). With decreased η, the band gap reduces until a Dirac point is formed when $\eta = \Delta$. Further decrease of η reopens the gap. This gap closing and reopening process is associated with band inversion, as the parities between the middle two bands exchange signs. When $\eta < \Delta$, the system enters the Kitaev phase and MESs emerge (figure 2(b)). When η becomes negative and $|\eta| < \Delta$, the parities of the top two bands as well as the bottom two bands exchange signs, and the system remains in the Kitaev phase (figure 2(c)). When η is further reduced with $|\eta| > \Delta$, the parities of the top two bands become '+' and the bottom two bands are '−', so that the system becomes the SSH-like topological phase (figure 2(d)). Consequently, three distinct topological phases can be achieved by tuning the capacitance in the circuit, including the trivial phase, Kitaev phase and SSH topological phase.

To further confirm the distinct topology of the three phases, we constructed a finite LC circuit consisting of 200 unit cells and calculated the discrete energy levels, which are presented in figures 2(e)–(h). For the trivial phase, there are no gap states inside the bulk gap, indicating trivial topology (figure 2(e)). When the circuit is in the Kitaev phase, two degenerate in-gap states can be clearly identified, which can be assigned to MESs (figures 2(f) and (g)). For the SSH topological phase, four degenerate edge states exist within the gap (figure 2(h)), as each MES consists of two edge states.

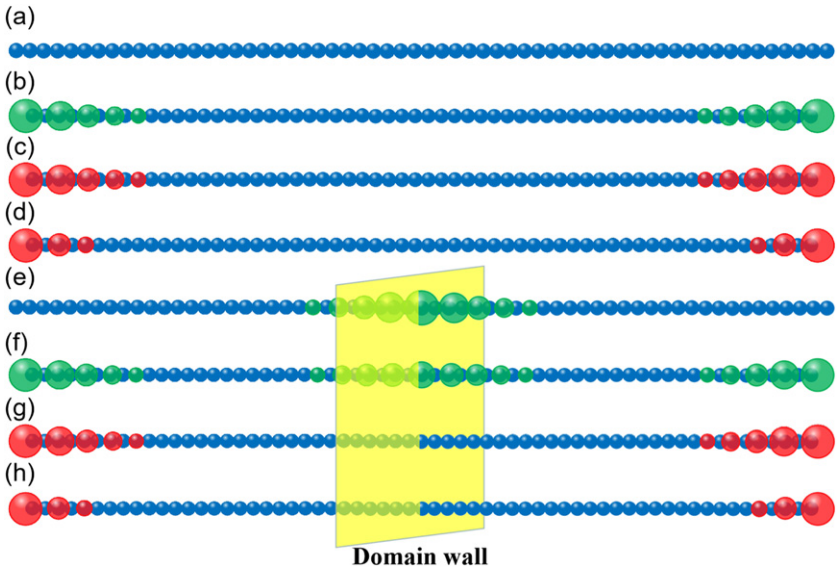

Figure 3. Field distribution of a finite circuit chain with different structures. Red and green colors represent MESs and SSH-like end states respectively, and size indicates the field strength. (a)–(d) Field strength distribution of a finite circuit chain with 200 unit cells under an excitation frequency set to the edge states, (a) the trivial phase with $\eta = 0.2$, (b) SSH topological phase with $\eta = -0.2$, (c) Kitaev phase with $\eta = 0.05$, and (d) Kitaev phase with $\eta = -0.05$. For all cases, $\Delta = 0.1$. (e)–(h) Same as (a)–(d) with a domain wall introduced in the middle of the chain.

3.2. MESs and topological phase transition

In electrical circuits, it is convenient to measure the field strength distribution of topological states in real space. We calculated field strength distribution of the finite LC circuit, as defined by $U_n = \sum_q |U_{n,q}|$, with $q = A, B, A^*$ and B^*, and present the results in figure 3. In the trivial phase, no field strength can be observed throughout the circuit chain (figure 3(a)). In the SSH topological phase, obvious edge states appear at the two ends of the chain (figure 3(b)). The Kitaev phase exhibits MESs at the two ends (figures 3(c) and (d)), and the difference between SSH edge states and MESs lies in their drastically different response towards grounding capacitors (analog to chemical potential), for which the SSH edge states are sensitive to the grounding capacitors, while MESs maintain robust (see figures S2 and S3 in note III). We further introduced a domain wall to the finite chain to explore the possible existence of solitons. Here, the domain wall refers to a point defect in the dimerized pattern, where we have added a pair of extra B-type inductors in the circuit chain. As shown in figures 3(e) and (f), solitons appear around the domain wall in SSH-like trivial and nontrivial phases, while there are no solitons in the Kitaev phase besides the MESs at two ends (figures 3(g) and (h)). Therefore, the field strength distribution provides valuable information on the topological states in real space, which should greatly benefit experimental characterization.

Topological phase transition has been extensively studied in condensed matter physics [42–44]. However, given a fixed structure, it is rather difficult to actively control and measure the phase transition. Topolectrical circuits hold advantages in a sense that the physical properties can be readily controlled by tuning the inductance and capacitance of the electrical components [31–35]. In this regard, we investigated the topological phase transition of the designed circuit by varying the capacitance (so that the superconducting pairing Δ can be tuned). Figure 4(a) shows the field strength distribution with respect to Δ and site index. As discussed above, when Δ is smaller than the hopping term η, the system is in the SSH trivial phase, where a soliton with a peak of field strength is observed around the domain wall. Decrease of Δ narrows the band gap and at $\Delta = \eta$, the gap closes with field strength spreading all over the chain. When $\Delta > \eta$, the system enters Kitaev phase, so that the soliton disappears and MESs emerge with two peaks localized at the two ends of chain. Tracing the whole process, it is easy to identify the Majorana splitting, where the field strength peak around the domain wall splits into two peaks at the ends. This provides an excellent signal of the topological phase transition.

To facilitate the observation of Majorana splitting in electrical circuit, we proposed an experimental observable, i.e., edge distance, as defined by, $d_{\text{edge}} = \sum_i (d_i \times \frac{U_i}{\sum_i U_i})$. d_{edge} represents the field strength weighted average distance from the nearest edge (d_i), so it is closely related to the field strength distribution. For a finite circuit chain with 200 unit cells, the peak around the domain wall corresponds to $d_{\text{edge}} \sim 100$ and the two peaks at the ends correspond to $d_{\text{edge}} \sim 0$. We plot the edge distance as a function of Δ in figure 4(b). It can be seen that the edge distance reduces monotonously with the increase of Δ, which provides an efficient observable to characterize the premonition of Majorana splitting in real experiments.

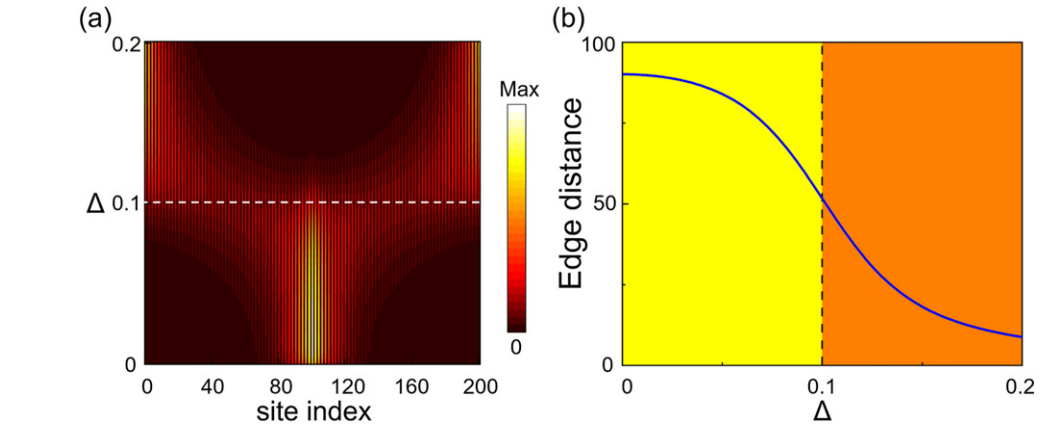

Figure 4. Illustration of Majorana splitting. (a) Illustration of the field strength distribution of a finite LC chain with a domain wall. Majorana splitting is indicated by the dashed horizontal line. (b) The proposed experimental observable, edge distance, as a function of Δ.

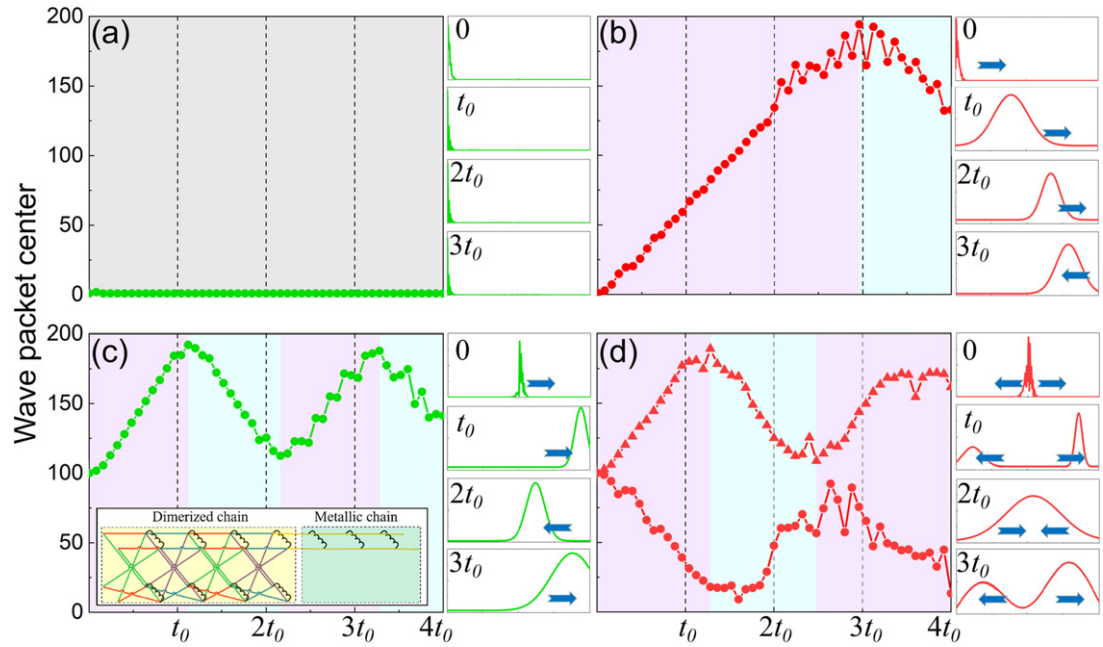

Figure 5. Dynamics in time domain. Time evolution of the Gaussian wave packet for a finite circuit chain with 200 unit cells in (a) SSH topological phase and (b) Kitaev phase. Figures on the right are the snapshots of propagation process with blue arrow indicating the traveling direction. (c) and (d) Same as (a) and (b) for a circuit heterostructure. Inset shows the configuration of the circuit heterostructure.

3.3. Dynamics in time domain

We further investigated the dynamics of the topological states in time domain to understand the different behaviors of SSH edge states and MESs under external excitation. For this purpose, we introduced a Gaussian wave packet in the finite circuit chain as well as in a constructed circuit heterostructure consisting of a finite circuit chain and a normal metal. The normal metal is simulated by an array of inductors connected by capacitors with the same capacitance without dimerization, and this metallic chain is connected to the upper array of the dimerized chain, as indicated in the insert of figure 5. The fourth Runge–Kutta method was used to explore the dynamics in time domain (more details in note IV).

The simulated time evolution of the Gaussian wave packet are shown in figure 5 and the supplementary videos. For the circuit chain in SSH topological phase, an excitation source at left end confines the Gaussian wave packet at the left, with no excitations extending into the bulk region (figure 5(a)), corresponding to metallic topological edge states and insulating bulk states. When the circuit chain is in the Kitaev phase, the wave packet propagates throughout the chain (figure 5(b)), consistent with the fact that MZMs behave non-locally [6]. For the constructed heterostructure with a finite circuit chain and a normal metal, an excitation source at the interface prevents the wave packet travelling into the circuit chain in the SSH

topological phase, so that the wave packet propagates only in the metal region (figure 5(c)). However, when the circuit chain is in Kitaev phase, the wave packet splits into two subpackets, which propagate in opposite directions simultaneously without influencing each other (figure 5(d)). This demonstrates that MESs in this circuit allow non-local propagation, exhibiting the non-local properties of real MZMs, while the edge states of SSH topological phases are strongly localized at the ends. In sharp contrast, the dynamics for non-topological scenarios behave as a normal insulator (figure S4). Besides, we have also calculated the dynamics in the presence of capacitance/inductance randomness and parasitic/contact resistances, and found that the topological modes can still be observed in practical experiments (see figure S5 in the supporting information). We believe that this signature is significant for facilitating the detection of MESs in topolectrical circuit.

4. Conclusion

In summary, we have demonstrated the implementation of dimerized Kitaev topolectrical circuit for the realization of MESs by using inductors and capacitors. The 1D dimerized Kitaev chain is successfully modeled by arranging two arrays of inductors for particles and antiparticles, while hopping and superconducting pairing are simulated by intra- and inter-array capacitive connections. Three distinct phases can be obtained by tuning the capacitance, including the trivial phase, SSH topological phase and Kitaev phase, which exhibit different field strength distributions in real space. Majorana splitting is observed during the topological phase transition from trivial to Kitaev phase, where the field strength peak at the domain wall splits into two peaks at two ends, and can be detected by an experimental observable-edge distance. We highlight the dynamics of Gaussian wave packets in time domain, as only MESs allow nonlocal propagation along the circuit. With high flexibility and tunability, our proposed topolectrical circuit not only provides an ideal platform for MESs, but also holds significant potential for future electrical engineering and signal processing applications. Meanwhile, the presented model is general, and can be applicable to other physical systems like photonic [45, 46], acoustic [47, 48], polaritonic [49] and mechanical systems [50]. Considering the rapid developments of this discipline [51–56], we believe that our work will stimulate considerable attention in a broad range of scientific and engineering communities.

Acknowledgments

This work was supported by the Natural Science Foundation of Zhejiang Province (LZ22A040004), the Science Challenge Project (TZ2018004), the National Natural Science Foundation of China (11674042), and the Thousand Youth Talents Program of China. We also acknowledge the support from the Center for High Performance Computing of Beihang University (BHHPC) and the Supercomputing Center of Zhongfa Aviation University.

Data availability statement

All data that support the findings of this study are included within the article (and any supplementary files).

Conflict of interest

The authors declare no conflict of interest.

ORCID iDs

Miao Zhou https://orcid.org/0000-0003-1390-372X

References

[1] Hasan M Z and Kane C L 2010 Colloquium: topological insulators *Rev. Mod. Phys.* **82** 3045–67
[2] Qi X-L and Zhang S-C 2011 Topological insulators and superconductors *Rev. Mod. Phys.* **83** 1057–110
[3] Young S M, Zaheer S, Teo J C Y, Kane C L, Mele E J and Rappe A M 2012 Dirac semimetal in three dimensions *Phys. Rev. Lett.* **108** 140405
[4] Burkov A A and Balents L 2011 Weyl semimetal in a topological insulator multilayer *Phys. Rev. Lett.* **107** 127205
[5] Hu J *et al* 2016 Evidence of topological nodal-line fermions in ZrSiSe and ZrSiTe *Phys. Rev. Lett.* **117** 016602
[6] Alicea J 2012 New directions in the pursuit of Majorana fermions in solid state systems *Rep. Prog. Phys.* **75** 076501

[7] Nayak C, Simon S H, Stern A, Freedman M and Das Sarma S 2008 Non-abelian anyons and topological quantum computation *Rev. Mod. Phys.* **80** 1083
[8] Oreg Y and von Oppen F 2020 Majorana zero modes in networks of Cooper-pair boxes: topologically ordered states and topological quantum computation *Annu. Rev. Condens. Matter Phys.* **11** 397
[9] Fu L and Kane C L 2008 Superconducting proximity effect and Majorana fermions at the surface of a topological insulator *Phys. Rev. Lett.* **100** 096407
[10] Fu L and Kane C L 2009 Josephson current and noise at a superconductor/quantum-spin-hall-insulator/superconductor junction *Phys. Rev.* B **79** 161408
[11] Cook A and Franz M 2011 Majorana fermions in a topological-insulator nanowire proximity-coupled to ans-wave superconductor *Phys. Rev.* B **84** 201105
[12] Sau J D, Lutchyn R M, Tewari S and Sarma S D 2010 Generic new platform for topological quantum computation using semiconductor heterostructures *Phys. Rev. Lett.* **104** 040502
[13] Alicea J 2010 Majorana fermions in a tunable semiconductor device *Phys. Rev.* B **81** 125318
[14] Lutchyn R M, Sau J D and Sarma S D 2010 Majorana fermions and a topological phase transition in semiconductor heterostructures *Phys. Rev. Lett.* **105** 077001
[15] Chung S B, Zhang H-J, Qi X-L and Zhang S-C 2011 Topological superconducting phase and Majorana fermions in half-metal/superconductor heterostructures *Phys. Rev.* B **84** 060510
[16] Ren H *et al* 2019 Topological superconductivity in a phase-controlled Josephson junction *Nature* **569** 93–8
[17] Vazifeh M M and Franz M 2013 Self-organized topological state with Majorana fermions *Phys. Rev. Lett.* **111** 206802
[18] Pientka F, Glazman L I and von Oppen F 2013 Topological superconducting phase in helical Shiba chains *Phys. Rev.* B **88** 155420
[19] Mourik V, Zuo K, Frolov S M, Plissard S R, Bakkers E P A M and Kouwenhoven L P 2012 Signatures of Majorana fermions in hybrid superconductor–semiconductor nanowire devices *Science* **336** 1003–7
[20] Rokhinson L P, Liu X and Furdyna J K 2012 The fractional a.c. Josephson effect in a semiconductor–superconductor nanowire as a signature of Majorana particles *Nat. Phys.* **8** 795–9
[21] Deng M T, Yu C L, Huang G Y, Larsson M, Caroff P and Xu H Q 2012 Anomalous zero-bias conductance peak in a Nb-InSb nanowire-Nb hybrid device *Nano Lett.* **12** 6414–9
[22] Churchill H O H, Fatemi V, Grove-Rasmussen K, Deng M T, Caroff P, Xu H Q and Marcus C M 2013 Superconductor-nanowire devices from tunneling to the multichannel regime: zero-bias oscillations and magnetoconductance crossover *Phys. Rev.* B **87** 241401
[23] Das A, Ronen Y, Most Y, Oreg Y, Heiblum M and Shtrikman H 2012 Zero-bias peaks and splitting in an Al-InAs nanowire topological superconductor as a signature of Majorana fermions *Nat. Phys.* **8** 887–95
[24] Finck A D K, Van Harlingen D J, Mohseni P K, Jung K and Li X 2013 Anomalous modulation of a zero-bias peak in a hybrid nanowire-superconductor device *Phys. Rev. Lett.* **110** 126406
[25] Albrecht S M, Higginbotham A P, Madsen M, Kuemmeth F, Jespersen T S, Nygård J, Krogstrup P and Marcus C M 2016 Exponential protection of zero modes in Majorana islands *Nature* **531** 206–9
[26] Yang Z, Heischmidt B, Gazibegovic S, Badawy G, Car D, Crowell P A, Bakkers E P A M and Pribiag V S 2020 Spin transport in ferromagnet-InSb nanowire quantum devices *Nano Lett.* **20** 3232–9
[27] van Zanten D M T *et al* 2020 Photon-assisted tunnelling of zero modes in a Majorana wire *Nat. Phys.* **16** 663–8
[28] Deng M T, Vaitiekėnas S, Hansen E B, Danon J, Leijnse M, Flensberg K, Nygård J, Krogstrup P and Marcus C M 2016 Majorana bound state in a coupled quantum-dot hybrid-nanowire system *Science* **354** 1557–62
[29] Shabani J *et al* 2016 Two-dimensional epitaxial superconductor–semiconductor heterostructures: a platform for topological superconducting networks *Phys. Rev.* B **93** 155402
[30] Karzig T *et al* 2017 Scalable designs for quasiparticle-poisoning-protected topological quantum computation with Majorana zero modes *Phys. Rev.* B **95** 235305
[31] Ezawa M 2019 Braiding of Majorana-like corner states in electric circuits and its non-Hermitian generalization *Phys. Rev.* B **100** 045407
[32] Lee C H, Imhof S, Berger C, Bayer F, Brehm J, Molenkamp L W, Kiessling T and Thomale R 2018 Topolectrical circuits *Commun. Phys.* **1** 39
[33] Rafi-Ul-Islam S M, Bin Siu Z and Jalil M B A 2020 Topoelectrical circuit realization of a Weyl semimetal heterojunction *Commun. Phys.* **3** 72
[34] Hofmann T, Helbig T, Lee C H, Greiter M and Thomale R 2019 Chiral voltage propagation and calibration in a topolectrical Chern circuit *Phys. Rev. Lett.* **122** 247702
[35] Imhof S *et al* 2018 Topolectrical-circuit realization of topological corner modes *Nat. Phys.* **14** 925
[36] Song L, Yang H, Cao Y and Yan P 2020 Realization of the square-root higher-order topological insulator in electric circuits *Nano Lett.* **20** 7566
[37] Yao J, Hao X, Luo F, Jia Y and Zhou M 2020 Quadrupole topological phase and robust corner resonance in Kekulé hexagonal electric circuit *New J. Phys.* **22** 093029
[38] Wang Y, Price H M, Zhang B and Chong Y D 2020 Circuit implementation of a four-dimensional topological insulator *Nat. Commun.* **11** 2356
[39] Wakatsuki R, Ezawa M, Tanaka Y and Nagaosa N 2014 Fermion fractionalization to Majorana fermions in a dimerized Kitaev superconductor *Phys. Rev.* B **90** 014505
[40] Su W P, Schrieffer J R and Heeger A J 1979 Solitons in polyacetylene *Phys. Rev. Lett.* **42** 1698
[41] Kitaev A Y 2001 Unpaired Majorana fermions in quantum wires *Phys.-Usp.* **44** 131
[42] Collins J L *et al* 2018 Electric-field-tuned topological phase transition in ultrathin Na_3Bi *Nature* **564** 390–4
[43] Liu Q, Zhang X, Abdalla L B, Fazzio A and Zunger A 2015 Switching a normal insulator into a topological insulator via electric field with application to phosphorene *Nano Lett.* **15** 1222
[44] Liu H, Sun J-T, Cheng C, Liu F and Meng S 2018 Photoinduced nonequilibrium topological states in strained black phosphorus *Phys. Rev. Lett.* **120** 237403
[45] Haldane F D M and Raghu S 2008 Possible realization of directional optical waveguides in photonic crystals with broken time-reversal symmetry *Phys. Rev. Lett.* **100** 013904
[46] Mittal S, Orre V V, Zhu G, Gorlach M A, Poddubny A and Hafezi M 2019 Photonic quadrupole topological phases *Nat. Photon.* **13** 692

[47] Prodan E and Prodan C 2009 Topological phonon modes and their role in dynamic instability of microtubules *Phys. Rev. Lett.* **103** 248101
[48] Yang Z, Gao F, Shi X, Lin X, Gao Z, Chong Y and Zhang B 2015 Topological acoustics *Phys. Rev. Lett.* **114** 114301
[49] Karzig T, Bardyn C-E, Lindner N H and Refael G 2015 Topological polaritons *Phys. Rev.* X **5** 031001
[50] Huber S D 2016 Topological mechanics *Nat. Phys.* **12** 621
[51] Zou D, Chen T, He W, Bao J, Lee C H, Sun H and Zhang X 2021 Observation of hybrid higher-order skin-topological effect in non-Hermitian topolectrical circuits *Nat. Commun.* **12** 7201
[52] Kotwal T, Moseley F, Stegmaier A, Imhof S, Brand H, Kießling T, Thomale R, Ronellenfitsch H and Dunkel J 2021 Active topolectrical circuits *Proc. Natl Acad. Sci. USA* **118** e2106411118
[53] Lenggenhager P M *et al* 2021 Electric-circuit realization of a hyperbolic drum (arXiv:2109.01148)
[54] Pan N, Chen T, Sun H and Zhang X 2021 Electric-circuit realization of fast quantum search *Research* https://doi.org/10.34133/2021/9793071
[55] Lin J Y, Hu N C, Chen Y J, Lee C H and Zhang X 2017 Line nodes, Dirac points, and Lifshitz transition in two-dimensional nonsymmorphic photonic crystals *Phys. Rev.* B **96** 075438
[56] Ni X and Alù A 2021 Higher-order topolectrical semimetal realized via synthetic gauge fields *APL Photon.* **6** 050802